https://doi.org/10.5194/acp-2022-837
Preprint. Discussion started: 30 January 2023


Atmospheric Chemistry and Physics Discussions

# Characterization of dust-related new particle formation events based on long-term measurement in North China Plain

Xiaojing Shen[1], Junying Sun[1,2], Yangmei Zhang[1], Chunhong Zhou[1], Ke Gui[1], Wanyun Xu[1], Quan Liu[1], Junting Zhong[1], Can Xia[1,3], Xinyao Hu[1,4], Sinan Zhang[1,5], Jialing Wang[1], Shuo Liu[1], Jiayuan Lu[1], Xiaoye Zhang[1]

[1]State Key Laboratory of Severe Weather & Key Laboratory of Atmospheric Chemistry of CMA, Chinese Academy of Meteorological Sciences, Beijing, 100081, China.

[2]State Key Laboratory of Cryospheric Science, Northwest Institute of Eco-Environment and Resources, Chinese Academy of Sciences, Lanzhou, 730000, China.

[3]Nanjing University of Information Science & Technology, Nanjing, 210000, China

[4]University of Chinese Academy of Sciences, Beijing, 100049, China

[5] Shaanxi Meteorological Observatory, Xi'an, 710014, China

*Corresponding to:* X. J. Shen (shenxj@cma.gov.cn)

**Abstract.** Mineral dust is a major natural atmospheric aerosol that impacts the Earth's radiation balance. The significant scavenging process of fine particles by the strong wind during the dust provided a relatively pristine environment in which the occurrence of new particle formation (NPF) was less influenced by anthropogenic emissions. In this study, the NPF occurred following the dust event (dust-related NPF) and other normal days (other NPF events) were classified based on the long-term particle number size distribution (PNSD) in urban Beijing in spring from 2017 to 2021. By comparing the two types of NPF events, we estimated that anthropogenic emissions could contribute approximately 50% to the observed formation and 30% to the growth rates. Anthropogenic emissions played a more important role when nucleated particles grew into the sizes above 10 nm. We also assessed a severe dust storm that originated from Mongolia and swept over northern China on March 15–16, 2021. The maximum hourly mean $PM_{10}$ mass concentration reached 8000 μg $m^{-3}$ during the dust storm. Secondary sulfate formation was enhanced by mineral dust, which was also favored by elevated ozone concentrations. However, a downward trend of particle hygroscopicity was found during dust storms as compared with the polluted episode, resulting in an increasing trend of the critical diameter at different supersaturations (*ss*) where aerosols are activated as cloud condensation nuclei (CCN), although NPF occurred at approximately noon time when dust faded. The critical diameter was elevated by approximately 6% - 10% (ss = 0.2% and 0.7%) during the dust storm, resulting in a lower CCN activation ratio, especially at low supersaturation. Modifications of the nucleation and growth process, as well as the particle-size distribution and hygroscopicity by the dust, provide valuable information that reveals the underlying climate and air quality effects of Asian mineral dust.

https://doi.org/10.5194/acp-2022-837
Preprint. Discussion started: 30 January 2023


Atmospheric Chemistry and Physics Discussions

## 1 Introduction

New particle formation (NPF) events have been identified as a major particle source and can produce approximately 50% of the cloud condensation nuclei (CCN), which leads to significant but poorly quantified radiative forcing (Gordon et al., 2017; Yu and Luo, 2009). Several studies have reported that NPF events can occur globally, including in pristine, urban, rural, forest, mountaintop, and coastal environments (Bianchi et al., 2016; Dada et al., 2017; Jokinen et al., 2018; Kulmala et al., 2004; Shen et al., 2011). Unlike relatively clean regions, the nucleation and subsequent growth processes are complex in polluted urban environments, due to the incomplete understanding of the dynamics of nano-particles and clusters under highly polluted conditions (Cai and Jiang, 2017; Kulmala et al., 2017). It also remains challenges to quantify the contribution of NPF events to haze formation in China because it is difficult to separate aerosols from primary sources and gas-to-particle formation (Kulmala et al., 2022).

Mineral dust particles are another important aerosol type in the atmosphere that primarily originate from arid and semiarid regions. They can significantly affect the radiative balance of the Earth's system by scattering and absorbing solar radiation, as well as the formation and properties of clouds by acting as CCN and ice nuclei (DeMott et al., 2010; Liao and Seinfeld, 1998; Seinfeld and Pandis, 1998; Twohy et al., 2009). Modelling predicted that total particle concentration and CCN were reduced by approximately 20% and 10%, respectively, in the dust pollution plume in East Asia (Manktelow et al., 2010). Dust particles can also lead to radiative feedback in the planetary boundary layer and lift dust particles to higher altitudes (Liu et al., 2016). The heterogeneous reactions of mineral dust with trace gases in the atmosphere can alter the chemical and physical properties of aerosols, including particle hygroscopicity (Ge et al., 2015; Tang et al., 2017). Heterogeneous oxidation of $SO_2$ onto particles has been observed, and is an important mechanism for converting $SO_2$ into sulfate (Li et al., 2011). Several laboratory and field studies have focused on the formation of secondary aerosols on dust particles (Liu et al., 2013; Xu et al., 2020). Dust particles enhance the reactive surface areas, absorb trace gases (Ma et al., 2017), and can further modify the chemical composition of the particles. Previous studies have also shown that the secondary formation of inorganics on the dust surface can enhance solubility and hygroscopicity (Mori, 2003; Perry et al., 2004).

In the economic developed and densely populated North China Plain (NCP) region, aerosols are dominated by anthropogenic emissions, and can cause serious air pollution (Zhang et al., 2019). However, a lidar study proved that approximately 45% of aerosols below 1.8 km above the ground are formed by polluted dust in Northern China (Wang et al., 2021). It has also been reported that the coarse mode (diameter ≥ 1 μm) serves as a medium and promotes rapid secondary aerosol formation, driving severe haze formation in the NCP region of China (Xu et al., 2020). However, the impact of dust bursts on nucleation and growth processes based on long-term measurement has not been discussed in urban areas in China based on open literature.

In this work, we analyzed NPF events based on long-term measurement of particle number size distribution (PNSD), to

https://doi.org/10.5194/acp-2022-837
Preprint. Discussion started: 30 January 2023


Atmospheric Chemistry and Physics Discussions

characterize NPF events influenced by dust. The occurrence of NPF events under clean conditions when the dust events fade facilitated the study of NPF events at a proxy baseline state of the atmosphere. This study helps to evaluate the contribution of anthropogenic emissions to the nucleation and growth processes. Specifically, a case study of a typical NPF event occurring after a severe dust storm is discussed in detail. A severe sand and dust storm (SDS) hit North East Asia from March 15 to 16, 2021, sweeping from Mongolia, through most parts of North China, and the Korean Peninsula, causing widespread damage, severe air pollution, and low visibility. This dust storm has been reported to be the most intensive event over the last two decades based on satellite and ground-based observations (Gui et al., 2022). For this specific case, the influence of dust on the NPF event, including the number/volume size distribution, chemical composition, and hygroscopicity of submicron particles, as well as CCN-sized particles, was analyzed to reveal the underlying climate and air quality effects of a typical severe Asian mineral dust storm.

## 2 Methodology

### 2.1 Sampling site

The physical and chemical properties of the particles were measured on the roof of the Chinese Academy of Meteorological Sciences (CAMS) building on the Chinese Meteorological Administration campus. The site is located approximately 53 m above ground level in the western Beijing urban area between the second- and third- ring roads. A major road with heavy traffic to the west of the site indicates that the sampled air could be influenced by traffic emissions. More information on the site can be found in the following studies (Shen et al., 2019; Wang et al., 2018).

### 2.2 Instrumentation

Ambient aerosols were sampled through a $PM_{10}$ impactor with a total flow rate of 16.7 Lpm. Different aerosol instruments were applied, including a tandem scanning mobility particle sizer (TSMPS, TROPOS, Germany). TSMPS system consisting of two differential mobility analyzers (DMAs, TROPOS, Germany) and two condensation particle counters (CPCs, models 3772 and 3776, TSI Inc., St Paul, USA), were used to measure the particle number size distributions (PNSDs) of 3–850 nm in mobility diameter at the CAMS site from 2017 to 2021. In this study, as we focused on dust events concentrated in spring, the data from March, April, and May from 2017 to 2021 were analyzed. Due to the malfunction of CPC 3776, which measured the PNSDs below 40 nm, the data in spring 2020 were excluded as the formation and growth rate of NPF days could not be precisely identified.

During the extensive campaign in the spring of 2021, in addition to TSMPS, other instruments including an aerodynamic particle sizer (APS, model 3321, TSI Inc., USA), hygroscopicity tandem differential mobility analyzer (H-TDMA, TROPOS, Germany), and an aerodyne high-resolution time-of-flight aerosol mass spectrometer (HR-ToF-AMS, Aerodyne Research, Inc.,

https://doi.org/10.5194/acp-2022-837
Preprint. Discussion started: 30 January 2023


Atmospheric Chemistry and Physics Discussions

USA) shared a common inlet, and the relative humidity (RH) of the sample air was controlled below 30% with an automatic regenerating absorption aerosol dryer system. Particles with an aerodynamic diameter in the size range of 0.5–10 μm were derived using APS. Combined with TSMPS data, the PNSD can be used to calculate the surface and volume concentrations, assuming a spherical particle shape. However, owing to the non-sphericity of the dust particles, the surface area cannot be directly converted. Previous studies have also revealed that APS can undersize particles with irregular shapes (Cheng et al., 1990) and oversize dense particles (Barron, 1996), and may result in approximately 10–30% under-sizing of dust particles (Cheng et al., 1990).

The selected dry particle sizes were 50 and 100 nm for H-TDMA. Each diameter at the RH setting was scanned three times, and each scan took 10 min. The chemical composition of non-refractory $PM_1$, including organic components, sulfate, nitrate, ammonium, and chloride, was derived using HR-ToF-AMS with a 5-min resolution.

The mass concentrations of $PM_{2.5}$ and $PM_{10}$ at the selected air quality monitoring sites were derived from the China National Environment Monitoring Center (CNEMC, http://www.cnemc.cn, last access: October 25, 2022). Trace gases at the CAMS site were measured simultaneously using a set of online analyzers from the Thermo Electron Corporation (USA), including $SO_2$ (43 CTL), $O_3$ (49C), and $NO_2$ (42 CTL).

### 2.3 Calculations

#### 2.3.1 NPF classification, formation and growth rate

The classification of NPF events was based on the principles and methods presented by Dal Maso et al. (2005), in which a distinct new mode of particles (3 - 25 nm) had to appear in the size distribution of the nucleation mode and grow into larger diameters in the following hours after nucleation started. The parameters characterizing NPF events, observed formation rate at 3 nm ($J_{obs}$), growth rate ($GR$), as the condensation sink ($CS$) can be determined by the PNSD measurement, as suggested by (Kulmala et al., 2012).

$$J_3 = \frac{dN_{3-25}}{dt} + CoagS \times N_{3-25} + \frac{GR_{3-25}}{\Delta dp} \times N_{3-25} \quad (1)$$

where $CoagS$ is the coagulation sink and $GR_{3-25}$ is the growth rate from 3 nm to 25 nm. Further, $GR$ is defined as the diameter rate of change with time: $GR = (D_{p,2} - D_{p,1})/dt$ (nm $h^{-1}$), where $D_{p,1}$ and $D_{p,2}$ are the geometric mean diameters ($D_{p,g}$) when the nucleated particles start and stop growing, respectively. $D_{p,g}$ can be derived using lognormal fitting algorithms (Hussein et al., 2005).

#### 2.3.2 Oxidation ratio of secondary inorganics

The sulfur oxidation ratio (SOR) and nitrogen oxidation ratio (NOR) are often used to estimate secondary sulfate and nitrate formation via the reactions of $SO_2$ and $NO_2$ (Wu et al., 2020). SOR and NOR are defined as the molar ratios of sulfate and

https://doi.org/10.5194/acp-2022-837
Preprint. Discussion started: 30 January 2023


Atmospheric Chemistry and Physics Discussions

nitrate to total oxidized sulfur and nitrogen, respectively, and are calculated as follows:

$$SOR = \frac{n[SO_4^{2-}]}{n[SO_4^{2-}] + n[SO_2]} \quad (2)$$

$$NOR = \frac{n[NO_3^-]}{n[NO_3^-] + n[NO_2]} \quad (3)$$

where n represents the molar concentration.

#### 2.3.3 Correction of the dust particle diameter

The TSMPS system gives the PNSD as a function of mobility diameter ($D_p$), which can represent the volume equivalent diameter ($D_{p,ve}$) for the spherical particles. The aerodynamic diameter ($D_{p,a}$) given by APS can be converted to the mobility diameter by applying the particle density ($\rho$) and shape factor ($\chi$), which can be used to derive the entire particle size range (3–10 μm) (Hinds, 1999; Reid, 2003):

$$D_{p,ve} = D_{p,a}\sqrt{\chi\frac{1}{\rho}} \times \sqrt{\frac{C_c(D_{p,a})}{C_c(D_{p,ve})}} \quad (4)$$

where $C_c$ is the Cunningham slip correction factor, and $C_c(D_{p,a})$ nearly equals to $C_c(D_{p,ve})$ due to the particles derived by APS being in the continuum region. For bulk dust aerosols, a density of 2.5 g cm$^{-3}$ and a mean shape factor of 1.8, which ranged from 1.6 to 2.6, were applied in this study (Reid et al., 2008).

#### 2.3.4 Hygroscopicity parameter

The hygroscopic parameter ($\kappa$) can be calculated using the approximate expression suggested by (Petters and Kreidenweis, 2007):

$$\kappa_{htdma} = (HGF^3 - 1)\left(\frac{\exp\left(\frac{A}{D_{p,dry} \times HGF}\right)}{RH} - 1\right) \quad (5)$$

$$\kappa_{ccn} = \frac{4A^3}{27D_{p,crit}^3 ln^2 S_c} \quad (6)$$

$$A = \frac{4\sigma_{s/a}M_w}{RT\rho_w} \quad (7)$$

where $D_{p,dry}$ (100 nm) and HGF are the initial dry particle diameter and hygroscopic growth factor at RH (90%) measured by H-TDMA, $\rho_w$ is the density of water (1.0 g cm$^{-3}$), $M_w$ is the molecular weight of water, $\sigma_{s/a}$ is the surface tension of the water solution (0.0728 N m$^{-2}$), $R$ is the universal gas constant, $T$ is the temperature, and $D_{p,crit}$ is the critical value at which 50% of the particles are activated at supersaturation ($S_c$).

https://doi.org/10.5194/acp-2022-837
Preprint. Discussion started: 30 January 2023


Atmospheric Chemistry and Physics Discussions

## 3 Results and discussion

### 3.1 The overall dust-related NPF events from 2017 to 2021

The dust days were classified into three types based on visibility (National Weather Bureau of China, 1979; Wang et al., 2005), including dust storms with sand being lifted by strong winds and visibility (vis) < 1.0 km; blowing dust formed by wind carrying a lot of dust and sand, with visibility of 1.0-10 km, and floating dust with fine dust suspended in the lower troposphere with vis ≤ 10 km. From 2017 to 2021, dust storms, blowing dust, and floating dust occurred once on March 15 2021, 13 days, and 25 days, respectively. Following approximately 80% of the dust days, the NPF event subsequently occurred, as shown in Fig.1. Considering the total NPF days in each spring (March, April, May) from 2017 to 2021, there were 44 days in 2017, 29 days in 2018, 30 days in 2019 and 31 days in 2021. The abrupt outbreak of the coronavirus disease 2019 (COVID-19) in early 2020 and the preventive restrictions of human activity resulted in the reduction of anthropogenic emissions (Le et al., 2020). Besides the instrument malfunction as mentioned above, in order to exclude the influence of the COVID-19, NPF events in the spring of 2020 were not discussed in this study. However, we elucidated that the elevated atmospheric oxidizing capacity during the lockdown period favored nucleation and growth processes in urban Beijing (Shen et al., 2021).

With increasing wind speed during the dust period, dilution by the northerly clean air facilitated pre-existing particle dispersion and scavenging, which provided a proxy baseline state of the background atmospheric condition. The comparison of *CS* between the dust-related NPF and other NPF events (Fig. 2) showed that *CS* was much lower for the dust-related NPF events. The median *CS* of dust-related NPF and other NPF events were 0.007 $s^{-1}$ and 0.015 $s^{-1}$, respectively. This indicates a much lower pre-existing particle number (or surface) concentration, which could represent a background atmosphere. It should be noted that the *CS* calculation did not consider coarse mode particles. However, the influence of the dust particles on *CS* is minor based on the calculation in the following discussion.

Table 1. The date of different dust types observed in Beijing from 2017 to 2021

| Dust type | Date (yyyy-mm-dd) |
|---|---|
| Dust storm | 2021-03-15 |
| Blowing dust | 2017-05-04, 2017-05-05, 2017-05-11<br>2018-05-28<br>2019-3-29, 2019-4-18, 2019-11-17<br>2020-03-18, 2020-05-11<br>2021-03-28, 2021-04-15, 2021-05-06, 2021-05-07 |
| Floating dust | 2018-03-28, 2018-05-01, 2018-05-05 |

https://doi.org/10.5194/acp-2022-837
Preprint. Discussion started: 30 January 2023


Atmospheric Chemistry and Physics Discussions

| | |
|---|---|
| | 2019-02-05, 2019-03-18, 2019-03-20, 2019-03-27, 2019-04-05, 2019-05-12, 2019-05-15, 2019-10-28 |
| | 2020-04-24, 2020-05-13, 2020-10-21 |
| | 2020-10-31, 2021-01-13, 2021-01-15, 2021-02-21, 2021-02-22, 2021-03-30, 2021-03-31, 2021-04-01, 2021-04-16, 2021-05-08, 2021-05-23 |

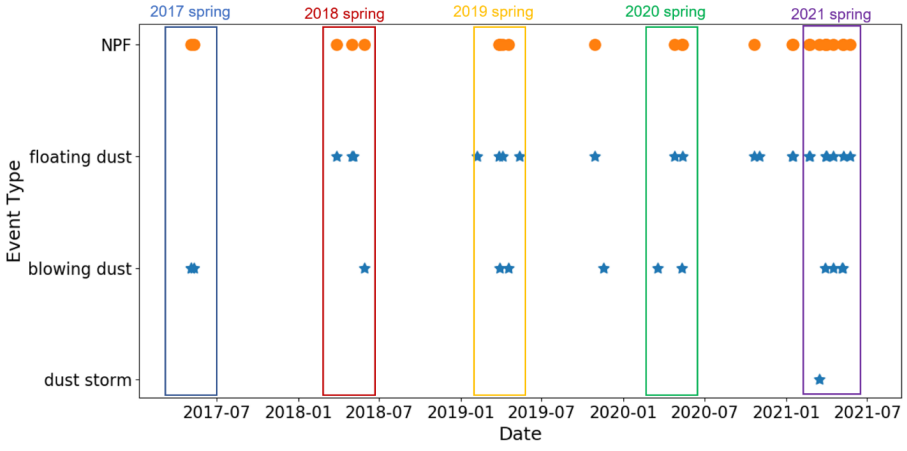


Fig.1 The occurrence of dust events, including dust storms, blowing dust, and floating dust from 2017 to 2021, and the NPF events observed after each dust event. The stars and dots represent the dust and NPF events, respectively.

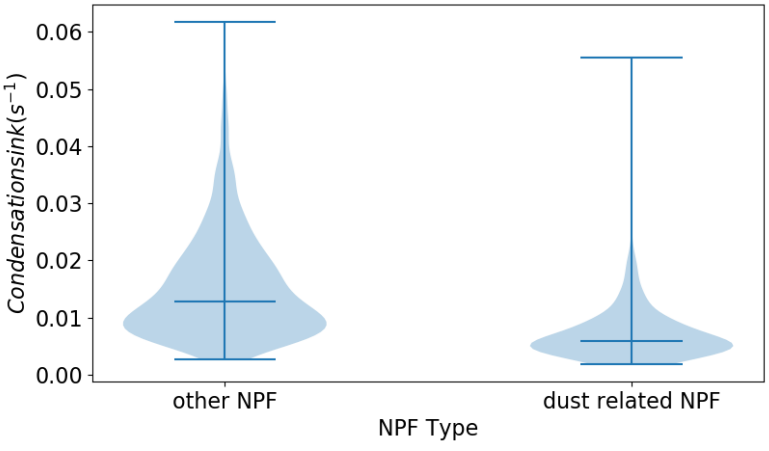


165

Fig. 2 The violin plot of condensation sink (*CS*) of dust-related NPF and other NPF events, the bars from bottom to top indicate the minimum, mean and maximum values, and the shaded area represents the distribution probability of the *CS*.

The anomaly plots were obtained by means of the PNSD of NPF occurring on non-dust days subtracting the mean PNSD of dust-related NPF in each spring from 2017 to 2021, and was shown in Fig. 3. Positive PNSD anomalies (Fig. 3a, c, e, g) in

https://doi.org/10.5194/acp-2022-837
Preprint. Discussion started: 30 January 2023


Atmospheric Chemistry and Physics Discussions

nucleation and Aitken mode showed stronger nucleation and growth processes. The calculated increase rates of nucleation mode particles according to the positive anomaly of PNSD, can be considered as the contribution by anthropogenic emissions Table 2 lists the statistical values of dust-related NPF events and other NPF events. The observed formation rate on dust-related NPF days ($J_{obs,dust\_NPF}$) accounted for approximately 43%-58% of the value on other NPF days ($J_{obs,other\_NPF}$) from 2017 to 2021, with a mean value of approximately 51%. *GR* of dust related-NPF ($GR_{dust\_NPF}$) ranged from 2.0 to 3.1 nm $h^{-1}$, whereas the value of other NPF days ($GR_{other\_NPF}$) was 3.6 to 4.3 nm $h^{-1}$. The fraction of $GR_{dust\_NPF}$ to $GR_{other\_NPF}$ ranged from 50% to 86%, with a mean value of approximately 67%. However, the growth process usually undergone several hours, with considerable anthropogenic emissions contributing to the particle growth. That indicated the influence by anthropogenic emission could explain no more than 33% of the growth process.

Table 2. The statistical values of NPF in spring from 2017-2021, including the number (*N*) of dust related NPF events, other NPF events and observed formation rate ($J_{obs}$), and growth rate (*GR*) of these two types NPF events

| | Spring 2017 | Spring 2018 | Spring 2019 | Spring 2021 |
|---|---|---|---|---|
| $N_{dust\_NPF}$ | 2 | 3 | 4 | 8 |
| $N_{other\_NPF}$ | 42 | 26 | 26 | 23 |
| $J_{obs,dust\_NPF}$ ($cm^{-3}$ $s^{-1}$) | 1.5±0.2 | 3.3±2.1 | 4.6±2.4 | 3.8±1.0 |
| $J_{obs,other\_NPF}$ ($cm^{-3}$ $s^{-1}$) | 3.3±2.6 | 7.3±4.8 | 8.1±4.5 | 6.7±3.2 |
| $GR_{dust\_NPF}$ (nm $h^{-1}$) | 2.0±0.6 | 2.9±0.3 | 3.1±0.5 | 2.8±1.2 |
| $GR_{other\_NPF}$ (nm $h^{-1}$) | 4.0±1.6 | 4.4±2.0 | 3.6±1.5 | 4.3±1.9 |

https://doi.org/10.5194/acp-2022-837
Preprint. Discussion started: 30 January 2023


Atmospheric Chemistry and Physics Discussions

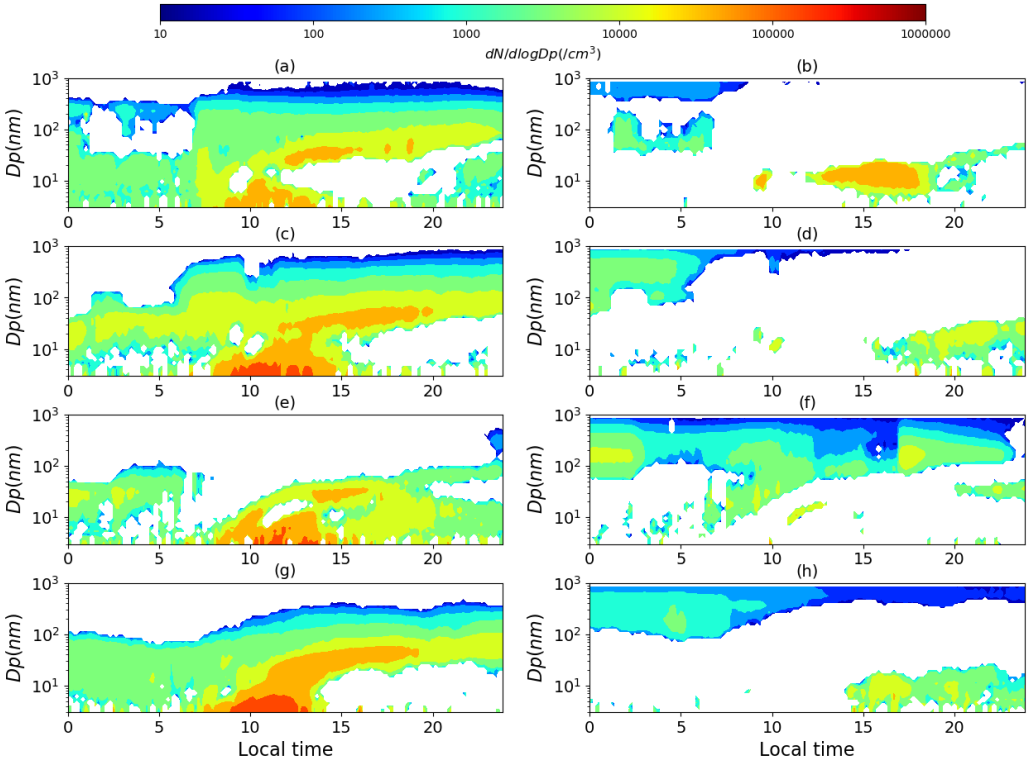


Fig. 3 The positive (a, c, e, g) and negative (b, d, f, h) anomalies of PNSD derived by the mean PNSDs of NPF events on non-dust days in spring (March, April, and May) subtracting the means of dust-related NPF days in 2017 (a, b), 2018 (c, d), 2019 (e, f) and 2021 (g, h).

The concentration of particles in the size range of 3–10 nm ($N_{3\text{-}10}$) and 3–25 nm ($N_{3\text{-}25}$) on dust-related NPF days and other NPF days is shown in Fig. 4. $N_{3\text{-}10}$ and $N_{3\text{-}25}$ were generally lower on dust-related NPF days than on other NPF days, indicating a considerable contribution by anthropogenic emissions. The mean ratios of $N_{3\text{-}10}$ and $N_{3\text{-}25}$ on dust NPF days compared to the value on other NPF days were 0.58 and 0.52, respectively, and were comparable with fraction caused by the anthropogenic emissions to the $J_{obs}$, as discussed above. $D_{p,g}$, derived from mean PNSD on dust-related NPF days and other NPF days, is shown in Fig. 5. It also showed a much lower $D_{p,g}$ on dust-related NPF days, especially at the initial growth stage when $D_{p,g}$ was below 10 nm. At the subsequent growth stage ($D_{p,g} > 10$ nm), the ratio of $D_{p,g}$ on dust-related NPF days compared to that on other NPF days was 0.52 to 0.58, except in spring in 2019. This indicated that the contribution of anthropogenic emissions to the growth process was approximately 40–50%, which was generally higher than the influence on the *GR* calculation, as discussed above. Specifically, the influence of anthropogenic emitted precursors when nucleated particles growing into the sizes above 10 nm was more significant. However, the contribution from anthropogenic emissions could be underestimated, as even during the growth process of dust-related NPF events, freshly-emitted precursors could also participate.

https://doi.org/10.5194/acp-2022-837
Preprint. Discussion started: 30 January 2023


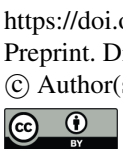

Atmospheric Chemistry and Physics Discussions

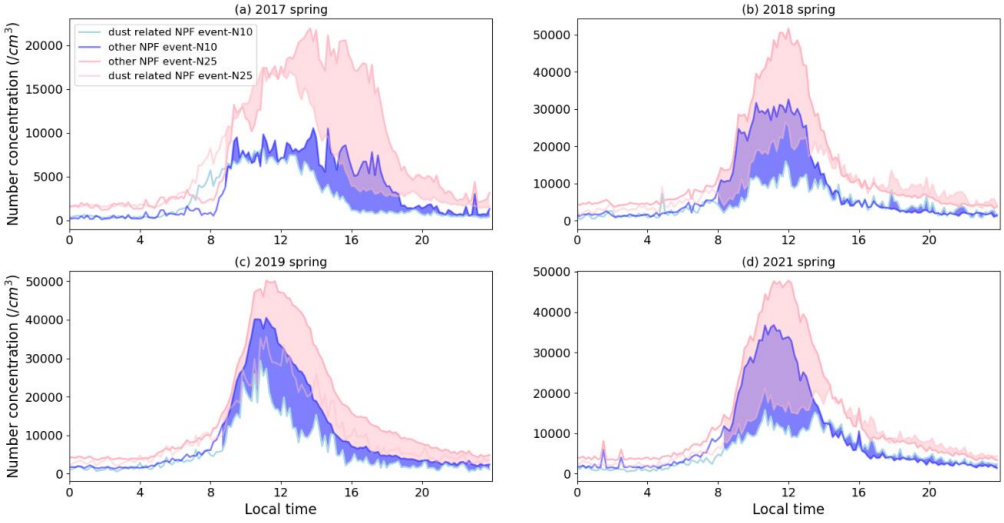


Fig. 4 Number concentration of particles below 10 nm ($N_{10}$) and 25 nm ($N_{25}$) of dust-related NPF events and other NPF events in spring in 2017 (a), 2018 (b), 2019 (c) and 2021 (d), respectively. The blue and pink shaded areas represent the anomaly of $N_{10}$ and $N_{25}$ between the two NPF event types during the nucleation process, respectively.

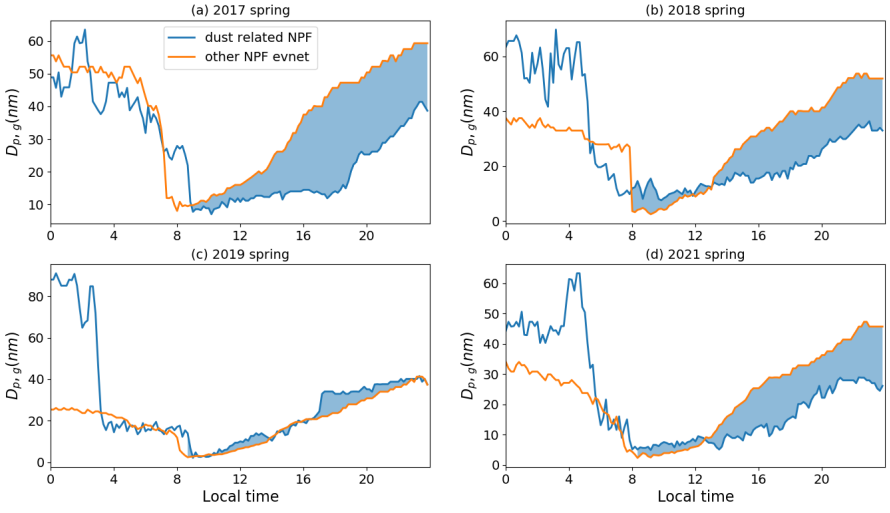


Fig. 5 Diurnal pattern of geometric mean diameter ($D_{p,g}$) of the PNSD derived by mean particle number size distribution of dust-related NPF events (blue line) and other NPF events (orange line) in spring (March, April, and May) in 2017 (a), 2018 (b), 2019 (c) and 2021 (d), respectively. The shaded area indicates the anomaly of $D_{p,g}$ during the nucleation and growth processed between the two NPF event types.

### 3.2 Size distribution of mineral dust

A severe dust storm that originated from Mongolia and swept through northern China on March 15, 2021, resulted in an

https://doi.org/10.5194/acp-2022-837
Preprint. Discussion started: 30 January 2023


Atmospheric Chemistry and Physics Discussions

extremely high particle mass concentration and low visibility. Four typical air quality monitoring sites, including Guanyuan (GY), Wanshou Temple (WST), Dongsi (DS), and Chaoyang (CY), in urban Beijing were selected to help understand the evolution of $PM_{2.5}$ and $PM_{10}$ mass concentrations during the dust storm (Fig. 6). The maximum of hourly mean $PM_{2.5}$ and $PM_{10}$ mass concentrations exceeded 600 and 8000 μg/m$^3$, respectively, at these selected sites which demonstrates the magnitude of this dust storm. The reported $PM_{10}$ mass concentration was the highest among the recent 20-year data in Beijing released by the CNEMC, as well as in Northern China. The $PM_{10}$ mass concentration was a magnitude higher than the value of $PM_{2.5}$, during the dust-dominated period of 8:00–18:00 local time (LT), indicating the major contribution of dust particles with size above 2.5 μm. From the PNSD plot in Fig. 7, it was found that particles above 400 nm started to increase on March 15 at 8:00 LT, indicating the arrival of dust particles. In the following two hours, the volume size distribution showed that concentration peaked in the size range of 8–10 μm. Based on the lognormal fitted parameters of the volume distribution, volume median mobility diameter ($D_{p,vol}$) was 8–10 μm during the initial stage (10:00–12:00 LT) of the dust storm and decreased to approximately 4–6 μm from 12:00 to 24:00 LT on March 15. It was comparable with previously reported values for other dust storms across the globe, ranging from 3.0 to 6.5 μm (Reid et al., 2008; Maring, 2003; Peters, 2006).

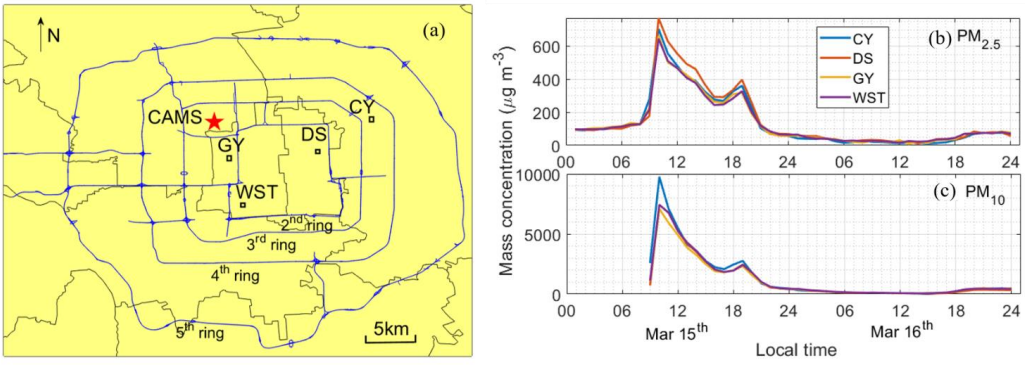


Fig. 6 The location map of CAMS site and four air quality monitoring sites, including Guanyuan (GY), Wanshou Temple (WST), Dongsi (DS), and Chaoyang (CY), in urban Beijing (a)

The dust storm weakened in the late afternoon of March 15, and NPF event occurred on the morning of March 16. During the polluted conditions before the dust storm (March 14), fine particles (diameter < 1 μm) dominated the particle number and mass concentration. However, coarse-mode particles contributed the most to the particle mass, volume, and surface concentration. In contrast to the NPF events occurring during the dust storm at Mt. Heng in South China (Nie et al., 2014), the NPF event on March 16 in this study occurred when dust particles vanished and there was a reduced *CS*. However, the NPF event was interrupted in the afternoon (~16:00 LT), which was influenced by the backflow of dust, as indicated by the elevated volume concentration as shown in Fig. 7b. The concentrations of $SO_2$ and $O_3$ increased in the morning of March 16, as shown in Fig. 8, indicating enhanced precursors and atmospheric oxidation capacity that favored NPF. Furthermore, metal

https://doi.org/10.5194/acp-2022-837
Preprint. Discussion started: 30 January 2023


Atmospheric Chemistry and Physics Discussions

photocatalysts in mineral dust can promote OH radial formation, which favors the conversion of $SO_2$ to $H_2SO_4$ during a nucleation event (Dupart et al., 2012).

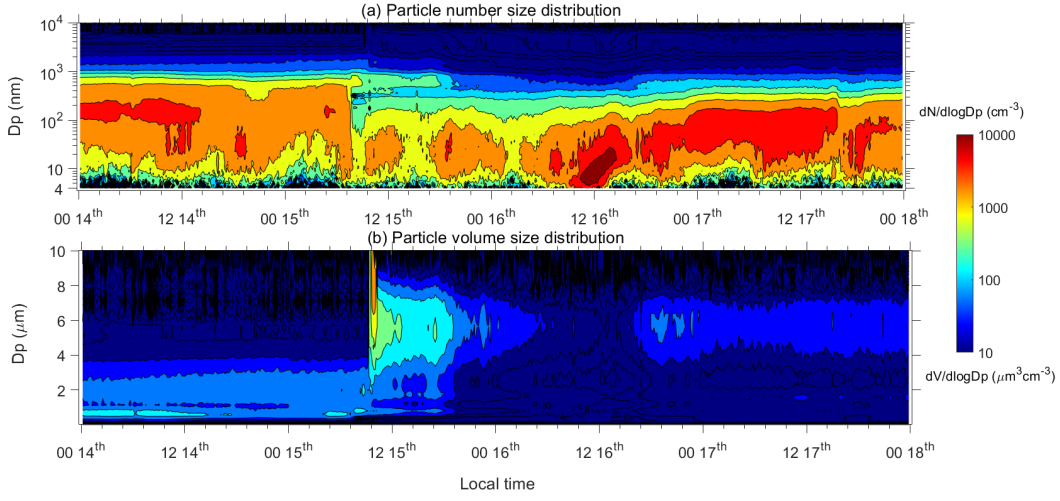


235 Fig. 7 Particle number (a) and volume (b) distributions on March 14–17, 2021, at CAMS station.

### 3.3 Secondary aerosol formation during dust storm

The variation in $NO_2$ sharply increased in the early morning (5:00–6:00 LT) on March 15, which could be attributed to the downward mixing of $NO_2$ rich air in the residual layer where $NO_2$ was trapped during the pollution episode on March 14 (Fig. 8). The increase in $NO_2$ and decrease in $O_3$ occurred at approximately 4:00 LT as the air masses changed from south to 240 northwest (Fig. S2 in Supplementary Materials). The concentration of $SO_2$ remained stable before 6:00 LT, probably because its distribution was uniform in the boundary layer. When the dust particles arrived in Beijing at 8:00 LT on March 15, the volume mixing ratio of $NO_2$ and $SO_2$ decreased immediately, which was also influenced by the enhanced aerosol surface uptake process owing to elevated particle surface concentration. Previous studies have revealed that the oxidation of $SO_2$ by ozone on the surface of mineral dust is an important pathway for sulfate formation (Ge et al., 2015; Usher et al., 2003). It has 245 also been reported that a dust event originated from the Gobi Desert and passed over northern and eastern China in 2014, and mixing occurred with anthropogenic emissions with high concentrations of $NO_2$ and promoted sulfate formation (Xie et al., 2015). However, the concentrations of $NO_2$ and $SO_2$ were low during dust storms, indicating that anthropogenic emissions had less influence. The concentration of $O_3$ increased during dust storms, probably because the $O_3$ budget was influenced by mineral dust. First, the photolysis of $O_3$ by ultraviolet radiation was weakened as the dust affected radiative fluxes and thus the 250 photolysis rate (Liao et al., 1999). Moreover, the heterogeneous processes occurring on dust particles may also change the $O_3$ budget by influencing the sources and sinks of $NO_2$ (Jacob, 2000). The volume mixing ratio of $NO_2$ decreased, while that of $O_3$ increased, indicating that the removal of $NO_2$ owing to heterogeneous uptake on the dust surface was helpful for the elevated $O_3$ concentration.

https://doi.org/10.5194/acp-2022-837
Preprint. Discussion started: 30 January 2023


Atmospheric Chemistry and Physics Discussions

As shown in Fig. 8, the $PM_1$ mass concentration derived from the AMS data showed high mass loading during the pollution episode (00:00–06:00 LT on March 15), with a mean value of 83.2 μg $m^{-3}$. Secondary inorganic aerosols were dominant, with nitrate being the major contributor, accounting for approximately 46% of the total particles. During the dust storm and post-dust period, $PM_1$ sharply decreased to approximately 5.0 μg $m^{-3}$, indicating a strong fine particle scavenging process by mineral dust. In contrast to the pollution episode, organics accounted for over 50%, with a larger mass fraction of primary organic aerosols (POA), approximately 40–60% of the organics during dust and post-dust storm periods. Under extremely clean conditions, secondary sulfate, nitrate, and ammonium (SNA) accounted for approximately 20%, 10%, and 15%, respectively. The chemical composition of fine particles changed from the dominant role of nitrate during the pollution episode to the largest contributor of organics during the dust storm. The decrease in $NO_2$ and nitrate suggests that they probably shifted from fine to coarse particles during dust storms (Wang et al., 2013). However, the sulfate mass fraction during dust and post-dust was higher than that during the pollution episode, indicating a higher formation process of secondary sulfate. From 5:00 LT on March 15 to 12:00 LT on March 16, the northwesterly air mass and local wind direction did not change (Figs. S1 and S2 in Supplementary Materials). The $SO_2$ volume mixing ratio increased quickly when the dust storm faded (22:00 LT on March 15), indicating that dust particles could be a major $SO_2$ sink (Usher et al., 2003). $NO_2$ also decreased when the dust storm started; however, it did not increase significantly when the dust storm ended, which differed from the variation in $SO_2$. This indicates different sinks for $SO_2$ and $NO_2$ during the dust storms. As discussed above, the uptake by mineral dust was a major sink for $SO_2$, whereas the uptake of $NO_2$ was minor, as the concentration remained low when the dust storm ended.

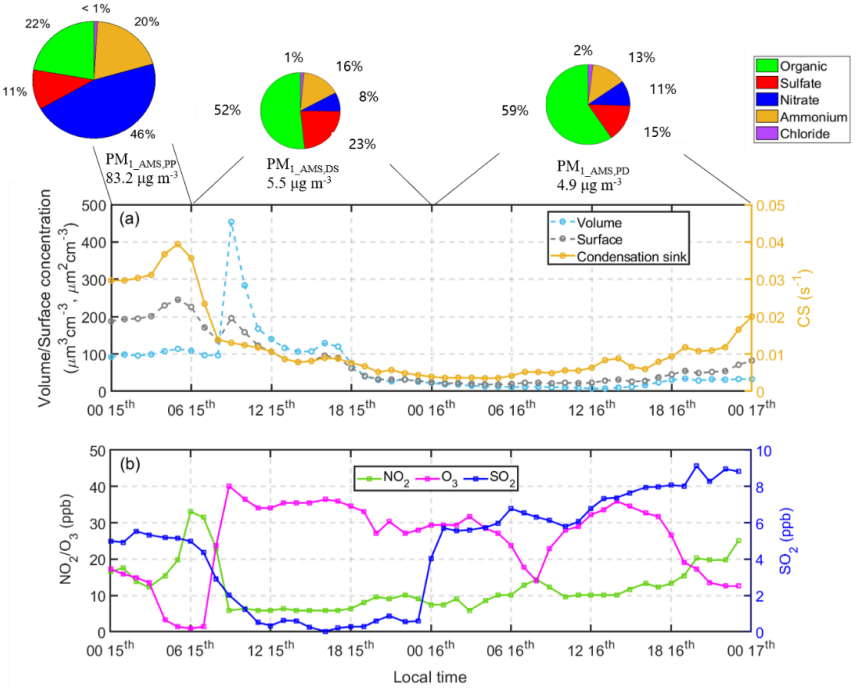

https://doi.org/10.5194/acp-2022-837
Preprint. Discussion started: 30 January 2023


Atmospheric Chemistry and Physics Discussions

Fig. 8 Time series of $PM_{10}$ volume, surface and condensation sink from March 15–17. Pollution period (PP), dust storm (DS) and post-dust (PD) are marked in the plot and the $PM_1$ mass concentration, as well as each chemical composition (organic, sulfate, nitrate, ammonium, and chloride) mass fraction is also given for each period (a), and hourly time series of $NO_2$, $O_3$ and $SO_2$ (b).

The oxidation ratios of $SO_2$ (SOR) and $NO_2$ (NOR) are shown in Fig. 9. It has been reported that the SOR was 0.18 in clean air conditions, whereas it was 0.27 under polluted conditions in Beijing in 2016 wintertime, indicating that $SO_2$ secondary transformation was a major pathway of sulfate production with a higher conversion efficiency under the polluted episode, whereas NOR was approximately 0.08, under both clean and polluted conditions (Wu et al., 2019). The SOR and NOR of $PM_1$ showed a clear positive relationship with the sulfate and nitrate mass concentrations, respectively, during the heavy dust period, as indicated by the volume mean diameter ($D_{p,vol}$) (Fig. 9). Although SOR and NOR were calculated based on the submicron particles and $D_{p,vol}$ represented the dust particles, their correlations could reflect how the heterogeneous reactions were modified by the dust (Usher et al., 2003). SOR ranged from 0.2 to 0.9 during the dust storm, which was even higher than the value during the polluted episode, approximately 0.3. During the dust storm period, transitional metal ions (TMIs) such as Fe(III) and Mn(II) can act as catalysts that favor sulfate formation via $SO_2$ oxidation (Usher et al., 2003). NOR showed a stronger positive relationship with nitrate mass concentration. However, the NOR was relatively low, with a value of 0.01–0.1, which was much lower than the value under polluted conditions, ranging from 0.3–0.5. This indicates that the dust particles promoted the secondary inorganic formation of submicron particles, particularly sulfate formation. Although the uptake and oxidation of $NO_2$ and $SO_2$ by mineral dust can be considerable, secondary aerosol formation in the submicron range is also important. As discussed above, it has been shown that $O_3$ increases during a dust storm (Fig. 8), which indicates enhanced oxidation capability during the dust storm and favors secondary inorganic aerosol formation by ozone oxidation. $O_3$ can also promote the heterogeneous oxidation of other trace gases on mineral dust surfaces (Li et al., 2006; Wu et al., 2011). Although the secondary formation of sulfate and nitrate was enhanced during the dust event, the $PM_1$ mass concentration, as well as each chemical component, decreased sharply owing to dilution by the strong wind during the dust storm.

https://doi.org/10.5194/acp-2022-837
Preprint. Discussion started: 30 January 2023


Atmospheric Chemistry and Physics Discussions

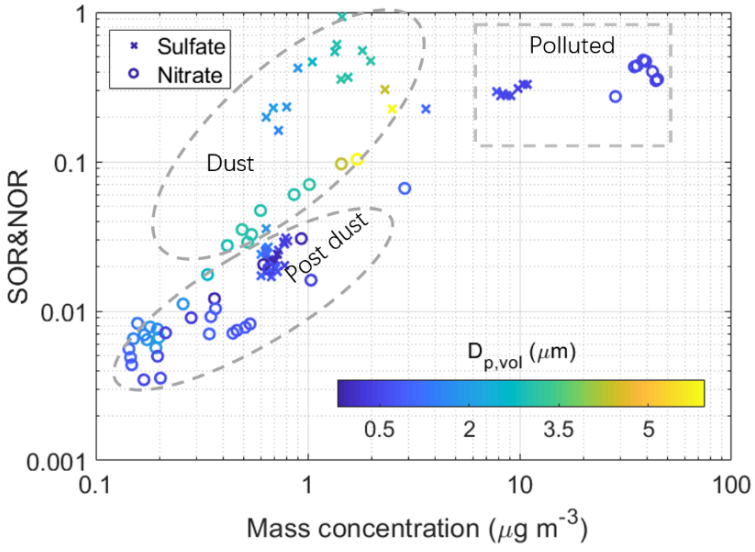


Fig. 9 Scatter plot of sulfate (cross) and nitrate (circle) mass concentrations in x-axis versus sulfur oxidation ratio (SOR) and nitrogen oxidation ratio (NOR) in y-axis with different volume weighted diameter ($D_{p,vol}$) indicated by the color bar. Dust, post-dust and polluted periods are marked by dashed lines, respectively.

### 3.4 Variations of particle hygroscopicity

Because RH was quite low during the dust storm, ranging from 10–20%, the hygroscopic growth process of the particles in the ambient environment could be ignored. However, as discussed above, the chemical composition of $PM_1$ derived from AMS changed significantly during the dust storm compared to the pollution episode. The calculated hygroscopic parameter, $\kappa$ values, of 50- and 100-nm particles were significantly higher during the pollution episode than during the dust and post-dust storm periods (Fig. 10). The variations in the hygroscopicity of the submicron particles can be explained by their chemical composition (Fig. 8). The mass fraction of organic aerosols with weak hygroscopicity accounted for approximately 20% a minor fraction of the particles during the pollution episode, whereas it increased to more than 50% during the dust storm and post-dust storm periods. Meanwhile, the fraction of hydrophobic POA increased during the dust storm and post-dust storm periods, as strong wind diluted the pre-existing particles, and the anthropogenic emission contribution was minor during the severe dust storm. Although sulfate formation was enhanced during the dust storm, as discussed above, with the larger mass fraction during the dust and post-dust storm periods, the smaller fraction of nitrate and higher fraction of organic aerosols (OA) resulted in weaker particle hygroscopicity during the dust and post-dust storm periods. This indicates that dust storms can modify the chemical composition of submicron particles, which influences their hygroscopic behavior and ability to be activated as CCN.

https://doi.org/10.5194/acp-2022-837
Preprint. Discussion started: 30 January 2023


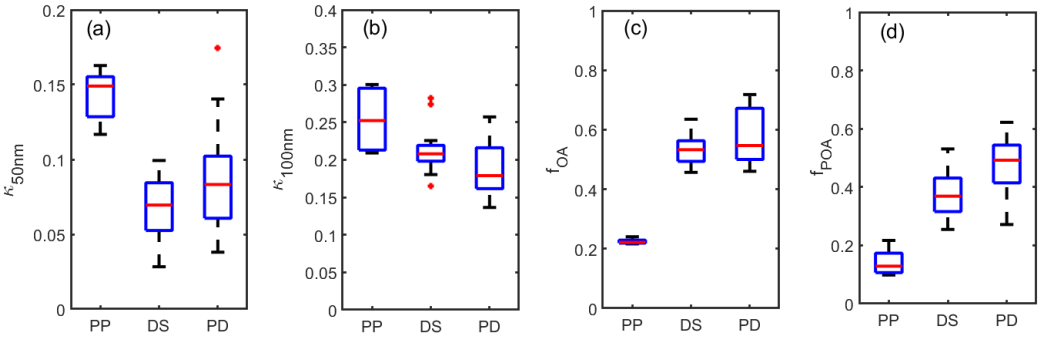


Fig. 10 Statistical boxplot of hygroscopic parameter ($\kappa$) of 50 (a) and 100 nm (b) and the mass fraction of organic aerosol (OA), $f_{OA}$ (c) accounting for $PM_1$, and mass fraction primary OA accounting for the organics, $f_{POA}$ (d) during the pollution (PP), dust (DS) and post-dust (PD) periods. The upper and lower boundaries of the box plots indicate the 75$^{th}$ and 25$^{th}$ percentiles, respectively, the line within the box marks the median, and the whiskers above and below the box indicate the 90th and 10th percentiles, respectively. Data points beyond the whiskers are displayed using a red cross.

### 3.5 Impact on the cloud condensation nuclei by the dust storm

Assume that $\kappa_{htdma} = \kappa_{ccn}$, $D_{p,crit}$ can be calculated based on Equations (6) and (7) on March 15 and 16, with a $\kappa$ value of 100 nm dry particles at a low or moderate cloud supersaturation ($S_c$) of 0.2% and a high $S_c$ of 0.7%. The $D_{p,crit}$ ranged from 45 to 60 nm at $S_c$ = 0.7%, with a mean value of 49 ± 2.5 nm, 52 ± 2.0 nm, and 53 ± 2.6 nm, during the polluted, dust, and post-dust storm periods, respectively, which were 112 ± 5.5 nm, 119 ± 6.5 nm, and 123 ± 7.2 nm, during the corresponding periods at $S_c$ = 0.2%. $D_{p,crit}$ increased during the dust storm and post-dust storm periods, by approximately 6% and 10%, respectively, compared with the pollution episodes. As $D_{p,crit}$ was larger than 45 nm, the number of particles larger than 45 nm ($CN_{45}$) was calculated and referred to as the potential CCN. The concentration of particles with diameters larger than $D_{p,crit}$ was calculated as the potential condensation nuclei ($CCN_{cal}$). The scatter plot of $CN_{45}$ and $CCN_{cal}$ under different conditions, indicated by the $D_{p,vol}$, as well as the activation ratio values ($R$) calculated by $CCN_{cal}$ dividing $CN_{45}$, are shown in Fig. 11. It shows $R$ values ranging from approximately 0.1 to 0.8 with $S_c$ = 0.2%, with higher values during polluted episodes (~0.8), lower values during the dust storm (0.2–0.4), and even reached 0.1–0.2 during the post-dust period. However, at high $S_c$ = 0.7%, $R$ values ranged from 0.6–1.0, and were close to 1.0, during the polluted episode, and concentrated around 0.8 during the dust episode. Results showed that the CCN activation capability was significantly influenced by the dust storm at a low $S_c$, whereas the influence was minor at a high $S_c$, depending on $D_{p,crit}$. Although an NPF event occurred during the post-dust period on March 16, $CCN_{cal}$ did not increase because of the elevated critical diameter. Moreover, as illustrated above, the NPF event was disrupted on the afternoon of March 16 and was affected by the backflow of dust. Although the floating dust particles did not result in clear increase of $PM_{2.5}$ and $PM_{10}$ mass concentration given in Fig. 6b, c, they induced a higher $CS$ (Fig. 8a), which was not favorable

https://doi.org/10.5194/acp-2022-837
Preprint. Discussion started: 30 January 2023


Atmospheric Chemistry and Physics Discussions

for the nucleation of particles growing to CCN-size.

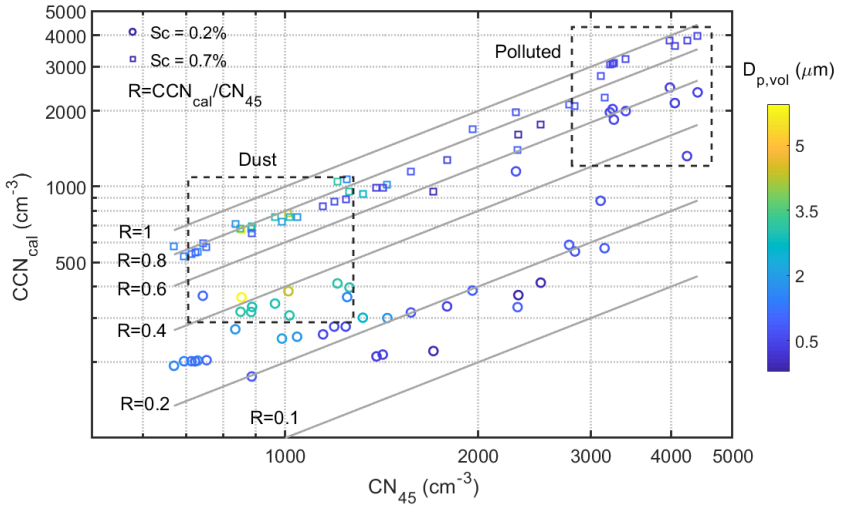


Fig. 11 Scatter plot of calculated cloud condensation nuclei ($CCN_{cal}$) under different supersaturations (Sc = 0.2% and 0.7%) and number concentration of diameter above 45 nm ($CN_{45}$), with different volume weighted diameter ($D_{p,vol}$) indicated by the colors. The solid lines representing the different ratio values between $CCN_{cal}$ and $CN_{45}$.

## 4 Conclusions

Dust days, including dust storms, blowing dust, and floating dust, have occurred frequently in the spring in recent years. We found there were approximately 80% of dust days followed by the NPF event based on the PNSD measurement in Beijing in spring from 2017 to 2021. Owing to the scavenging effect of strong winds on pre-existing aerosols, the occurrence of NPF after dust events could represent the minimum influence of anthropogenic emissions on the nucleation and growth processes. To study the effect of anthropogenic emissions on NPF events, the NPF events were classified into cases following dust (dust-related NPF) and other NPF events. Based on the PNSD derived on NPF days, it was found that anthropogenic emissions can contribute approximately 50% of the observed formation and 30% to the growth rates, and played a more important role for nucleated particles above 10 nm. However, the influence of anthropogenic emissions on the growth process of dust- related NPF events was not considered; thus, it was under estimated in the discussion.

The most severe mineral dust storm over the past two decades in China originated in Mongolia, and swept through northern China on March 15–16, 2021, with the highest hourly mean $PM_{10}$ reaching 8 mg $m^{-3}$, as observed in urban Beijing. The processes of mineral dust and their impact were evaluated based on field measurements of aerosols and reactive gases in urban Beijing. During dust storms, the volume-weighted particle size peaks at approximately 4–6 μm or 8–10 μm. The precursor gases ($SO_2$ and $NO_2$) were quickly scavenged by mineral dust, followed by conversion of the gases into secondary particles.

https://doi.org/10.5194/acp-2022-837
Preprint. Discussion started: 30 January 2023


Atmospheric Chemistry and Physics Discussions

In particular, secondary sulfate aerosol formation was found to have a higher rate than that of the polluted episode before the storm. The hygroscopicity of ultrafine particles was weakened during the dust and post-dust storm periods, as compared with the pollution episode, due to the elevated mass fraction of organics, especially the primary organic aerosols. Based on the $\kappa$-Köhler theory, the critical diameter of the particles activated as CCN was calculated for different supersaturations. They were approximately 49 nm and 112 nm in the polluted episode at $S_c$ of 0.7 and 0.2%, respectively, which increased to 52 nm and 119 nm, respectively, during the dust storm, increasing by approximately 6%. A new particle formation event occurred on March 16, when the dust vanished; however, it was interrupted by the backflow of float dust. As a consequence of the uptake of precursor gases on mineral dust, the physical and chemical properties of submicron particles changed, thereby influencing their ability to act as CCNs, especially at low supersaturation. The impact of this severe dust event observed in Beijing provided valuable information for evaluating the influence of dust, particularly the underlying impact of submicron particles and their ability to be activated as CCN. However, more work is needed to quantify the contribution of anthropogenic emissions to NPF based on field experiments and modelling work in the future.

## Acknowledgments

This research was supported by the National Natural Science Foundation of China (41875147, 42075082, 42090031), S&T Development Fund of CAMS (2020KJ001), Basic Research Fund of CAMS (2020Z002), and Innovation Team for Haze-fog Observation and Forecasts of MOST and CMA.

## Conflict of Interest

The authors declare no conflict interest.

## Open Research

All data used in the study are available from the corresponding author upon request (shenxj@cma.gov.cn).

## References

Criterion of Surface Meteorological Observation. Beijing, Meteorological Press National Weather Bureau of China, 1979.

Barron, P. A.: Calibration and use of the aerodynamic particle sizer (APS 3300), Aerosol Sci. Technol., 5: 55-67, 1996.

Bianchi, F., Trostl, J., Junninen, H., Frege, C., Henne, S., Hoyle, C. R., Molteni, U., Herrmann, E., Adamov, A., Bukowiecki, N., Chen, X., Duplissy, J., Gysel, M., Hutterli, M., Kangasluoma, J., Kontkanen, J., Kurten, A., Manninen, H. E., Munch, S., Perakyla, O., Petaja, T., Rondo, L., Williamson, C., Weingartner, E., Curtius, J., Worsnop, D. R., Kulmala, M., Dommen, J. and Baltensperger, U.: New particle formation in the free troposphere: A question of chemistry and timing, Science, 352(6289):

https://doi.org/10.5194/acp-2022-837
Preprint. Discussion started: 30 January 2023




1109-1112, DOI: 10.1126/science.aad5456, 2016.

Cai, R. and Jiang, J.: A new balance formula to estimate new particle formation rate: reevaluating the effect of coagulation scavenging, Atmospheric Chemistry and Physics, 17(20): 12659-12675, DOI: 10.5194/acp-17-12659-2017, 2017.

Cheng, Y. S., Chen, B. T. and Yeh, H. C.: Behavior of isometric nonspherical aerosol-particles in the aerodynamic particle sizer, J. Aerosol Sci., 21: 701– 710, 1990.

Dada, L., Paasonen, P., Nieminen, T., Buenrostro Mazon, S., Kontkanen, J., Peräkylä, O., Lehtipalo, K., Hussein, T., Petäjä, T., Kerminen, V.-M., Bäck, J. and Kulmala, M.: Long-term analysis of clear-sky new particle formation events and nonevents in Hyytiälä, Atmos. Chem. Phys., 17(10): 6227-6241, DOI: 10.5194/acp-17-6227-2017, 2017.

Dal Maso, M., Kulmala, M., Riipinen, I., Wagner, R., Hussein, T., Aalto, P. P. and Lehtinen, K. E. J.: Formation and growth of fresh atmospheric aerosols: Eight years of aerosol size distribution data from SMEAR II, Hyytiälä, Finland, Boreal Envrion. Res., 10: 323–336, 2005.

DeMott, P. J., Prenni, A. J., Liu, X., Kreidenweis, S. M., Petters, M. D., Twohy, C. H., Richardson, M. S., Eidhammer, T. and Rogers, D. C.: Predicting global atmospheric ice nuclei distributions and their impacts on climate, Proc Natl Acad Sci, 107(25): 11217-11222, DOI: 10.1073/pnas.0910818107, 2010.

Ge, M. F., Wu, L. Y., Tong, S. R., Liu, Q. F. and Wang, W. G.: Heterogeneous chemistry of trace atmospheric gases on atmospheric aerosols: An overview, Science Foundation in China, 23(3): 62-80, 2015.

Gordon, H., Kirkby, J., Baltensperger, U., Bianchi, F., Breitenlechner, M., Curtius, J., Dias, A., Dommen, J., Donahue, N. M., Dunne, E. M., Duplissy, J., Ehrhart, S., Flagan, R. C., Frege, C., Fuchs, C., Hansel, A., Hoyle, C. R., Kulmala, M., Kürten, A., Lehtipalo, K., Makhmutov, V., Molteni, U., Rissanen, M. P., Stozkhov, Y., Tröstl, J., Tsagkogeorgas, G., Wagner, R., Williamson, C., Wimmer, D., Winkler, P. M., Yan, C. and Carslaw, K. S.: Causes and importance of new particle formation in the present-day and preindustrial atmospheres, Journal of Geophysical Research: Atmospheres, 122(16): 8739-8760, DOI: 10.1002/2017jd026844, 2017.

Gui, K., Yao, W., Che, H., An, L., Zheng, Y., Li, L., Zhao, H., Zhang, L., Zhong, J., Wang, Y. and Zhang, X.: Record-breaking dust loading during two mega dust storm events over northern China in March 2021: aerosol optical and radiative properties and meteorological drivers, Atmos. Chem. Phys., 22(12): 7905-7932, DOI: 10.5194/acp-22-7905-2022, 2022.

Hinds, W. C., Aerosol Technology. New York 1999.

Jacob, D. J.: Heterogeneous chemistry and tropospheric ozone, Atmos. Environ., 34: 2131-2159, 2000.

Jokinen, T., Sipilä, M., Kontkanen, J., Vakkari, V., Tisler, P., Duplissy, E.-M., Junninen, H., Kangasluoma, J., Manninen, H. E., Petäjä, T., Kulmala, M., Worsnop, D. R., Kirkby, J., Virkkula, A. and Kerminen, V.-M.: Ion-induced sulfuric acid–ammonia nucleation drives particle formation in coastal Antarctica, Science Advance, 2018.

Kulmala, M., Cai, R., Stolzenburgb, D., Zhoua, Y., Dada, L., Guo, Y., Yan, C., Petäjä, T., Jiang, J. and Kerminen, V.-M.: The

https://doi.org/10.5194/acp-2022-837
Preprint. Discussion started: 30 January 2023




contribution of new particle formation and subsequent growth to haze formation, Environ. Sci.: Atmos., DOI: 10.1039/D1EA00096A, 2022.

Kulmala, M., Kerminen, V. M., Petaja, T., Ding, A. J. and Wang, L.: Atmospheric gas-to-particle conversion: why NPF events are observed in megacities?, Faraday Discuss, 200: 271-288, DOI: 10.1039/c6fd00257a, 2017.

Kulmala, M., Petäjä, T., Nieminen, T., Sipilä, M., Manninen, H. E., Lehtipalo, K., Dal Maso, M., Aalto, P. P., Junninen, H., Paasonen, P., Riipinen, I., Lehtinen, K. E. J., Laaksonen, A. and Kerminen, V.-M.: Measurement of the nucleation of atmospheric aerosol particles, Nature Protocols, 7(9): 1651-1667, DOI: 10.1038/nprot.2012.091, 2012.

Kulmala, M., Vehkamäki, H., Petäjä, T., Dal Maso, M., Lauri, A., Kerminen, V. M., Birmili, W. and McMurry, P. H.: Formation and growth rates of ultrafine atmospheric particles: a review of observations, J. Aerosol Sci., 35(2): 143-176, DOI: 10.1016/j.jaerosci.2003.10.003, 2004.

Le, T., Wang, Y., Liu, L., Yang, J., Yung, Y. L., Li, G. and Seinfeld, J. H.: Unexpected air pollution with marked emission reductions during the COVID-19 outbreak in China, Science, 10.1126/science.abb7431, 2020.

Li, J., Shang, J. and Zhu, T.: Heterogeneous reactions of $SO_2$ on ZnO particle surfaces, Science China Chemistry, 54(1): 161-166, DOI: 10.1007/s11426-010-4167-9, 2011.

Li, L., Chen, Z. M., Zhang, Y. H., Zhu, T., Li, J. L. and Ding, J.: Kinetics and mechanism of heterogeneous oxidation of sulfur dioxide by ozone on surface of calcium carbonate, Atmos. Chem. Phys., 6: 2453–2464, 2006.

Liao, H. and Seinfeld, J. H.: Radiative forcing by mineral dust aerosols: Sensitivity to key variables, J. Geophys. Res.: Atmospheres, 103(D24): 31637-31645, DOI: 10.1029/1998jd200036, 1998.

Liao, H., Yung, Y. L. and Seinfeld, J. H.: Effects of aerosols on tropospheric photolysis rates in clear and cloudy atmospheres, J. Geophys. Res.: Atmospheres, 104(D19): 23697-23707, DOI: 10.1029/1999jd900409, 1999.

Liu, C., Chu, B. W., Liu, Y. C., Ma, Q. X., Ma, J. Z., He, H., Li, J. H. and Hao, J. M.: Effect of mineral dust on secondary organic aerosol yield and aerosol size in α-pinene/NOx photo-oxidation, Atmos. Environ., 77: 781-789, DOI: 10.1016/j.atmosenv.2013.05.064, 2013.

Liu, L., Huang, X., Ding, A. and Fu, C.: Dust-induced radiative feedbacks in north China: A dust storm episode modeling study using WRF-Chem, Atmos. Environ., 129: 43-54, DOI: 10.1016/j.atmosenv.2016.01.019, 2016.

Ma, Q., Wang, T., Liu, C., He, H., Wang, Z., Wang, W. and Liang, Y.: $SO_2$ Initiates the Efficient Conversion of $NO_2$ to HONO on MgO Surface, Environ Sci Technol, 51(7): 3767-3775, DOI: 10.1021/acs.est.6b05724, 2017.

Manktelow, P. T., Carslaw, K. S., Mann, G. W. and Spracklen, D. V.: The impact of dust on sulfate aerosol, CN and CCN during an East Asian dust storm, Atmos. Chem. Phys., 10: 365–382, 2010.

Mori, I.: Change in size distribution and chemical composition of kosa (Asian dust) aerosol during long-range transport, Atmos. Environ., 37(30): 4253-4263, DOI: 10.1016/s1352-2310(03)00535-1, 2003.

https://doi.org/10.5194/acp-2022-837
Preprint. Discussion started: 30 January 2023




Perry, K. D., Cliff, S. S. and Jimenez-Cruz, M. P.: Evidence for hygroscopic mineral dust particles from the Intercontinental Transport and Chemical Transformation Experiment, J. Geophys. Res.: Atmospheres, 109(D23), DOI: 10.1029/2004jd004979, 2004.

Petters, M. D. and Kreidenweis, S. M.: A single parameter representation of hygroscopic growth and cloud condensation nucleus activity, Atmos. Chem. Phys., 7: 1961–1971, 2007.

Reid, J. S.: Comparison of size and morphological measurements of coarse mode dust particles from Africa, Journal of Geophysical Research, 108(D19), DOI: 10.1029/2002jd002485, 2003.

Reid, J. S., Reid, E. A., Walker, A., Piketh, S., Cliff, S., Al Mandoos, A., Tsay, S.-C. and Eck, T. F.: Dynamics of southwest Asian dust particle size characteristics with implications for global dust research, J. Geophys. Res., 113(D14), DOI: 10.1029/2007jd009752, 2008.

Seinfeld, J. and Pandis, S., Atmospheric Chemistry and Physics: From Air Pollution to Climate Change. Hoboken, New Jersey., John Wiley & Son, Inc, 1998.

Shen, X., Sun, J., Yu, F., Wang, Y., Zhong, J., Zhang, Y., Hu, X., Xia, C., Zhang, S. and Zhang, X.: Enhancement of nanoparticle formation and growth during the COVID-19 lockdown period in urban Beijing, Atmospheric Chemistry and Physics, 21(9): 7039-7052, DOI: 10.5194/acp-21-7039-2021, 2021.

Shen, X. J., Sun, J. Y., Zhang, X. Y., Zhang, Y. M., Zhong, J. T., Wang, X., Wang, Y. Q. and Xia, C.: Variations in submicron aerosol liquid water content and the contribution of chemical components during heavy aerosol pollution episodes in winter in Beijing, Sci Total Environ, 693: 133521, DOI: 10.1016/j.scitotenv.2019.07.327, 2019.

Shen, X. J., Sun, J. Y., Zhang, Y. M., Wehner, B., Nowak, A., Tuch, T., Zhang, X. C., Wang, T. T., Zhou, H. G., Zhang, X. L., Dong, F., Birmili, W. and Wiedensohler, A.: First long-term study of particle number size distributions and new particle formation events of regional aerosol in the North China Plain, Atmos. Chem. Phys., 11(4): 1565-1580, DOI: 10.5194/acp-11-1565-2011, 2011.

Tang, M., Huang, X., Lu, K. D., Ge, M. F., Li, Y. J., Cheng, P., Zhu, T., Ding, A. J., Zhang, Y. H., Gligorovski, S., Song, W., Ding, X., Bi, X. H. and Wang, X. M.: Heterogeneous reactions of mineral dust aerosol: implications for tropospheric oxidation capacity, Atmos. Chem. Phys., 17(19): 11727-11777, DOI: 10.5194/acp-17-11727-2017, 2017.

Twohy, C. H., Kreidenweis, S. M., Eidhammer, T., Browell, E. V., Heymsfield, A. J., Bansemer, A. R., Anderson, B. E., Chen, G., Ismail, S., DeMott, P. J. and Van Den Heever, S. C.: Saharan dust particles nucleate droplets in eastern Atlantic clouds, Geo. Res. Lett., 36(1), DOI: 10.1029/2008gl035846, 2009.

Usher, C. R., Michel, A. E. and Grassian, V. H.: Reactions on Mineral Dust, Chem. Rev., 103: 4883−4939, 2003.

Wang, G. H., Zhou, B. H., Cheng, C. L., Cao, J. J., Li, J. J., Meng, J. J., Tao, J., Zhang, R. J. and Fu, P. Q.: Impact of Gobi desert dust on aerosol chemistry of Xi'an, inland China during spring 2009: differences in composition and size distribution



between the urban ground surface and the mountain atmosphere, Atmos. Chem. Phys., 13(2): 819-835, DOI: 10.5194/acp-13-819-2013, 2013.

Wang, S., Wang, J., Zhou, Z. and Shang, K.: Regional characteristics of three kinds of dust storm events in China, Atmospheric Environment, 39(3): 509-520, DOI: 10.1016/j.atmosenv.2004.09.033, 2005.

Wang, X., Shen, X. J., Sun, J. Y., Zhang, X. Y., Wang, Y. Q., Zhang, Y. M., Wang, P., Xia, C., Qi, X. F. and Zhong, J. T.: Size-resolved hygroscopic behavior of atmospheric aerosols during heavy aerosol pollution episodes in Beijing in December 2016, Atmos. Environ., 194: 188-197, DOI: 10.1016/j.atmosenv.2018.09.041, 2018.

Wang, Z., Liu, C., Hu, Q., Dong, Y., Liu, H., Xing, C. and Tan, W.: Quantify the Contribution of Dust and Anthropogenic Sources to Aerosols in North China by Lidar and Validated with CALIPSO, Remote Sensing, 13(9), DOI: 10.3390/rs13091811, 2021.

Wu, L., Sun, J., Zhang, X., Zhang, Y., Wang, Y., Zhong, J. and Yang, Y.: Aqueous-phase reactions occurred in the PM2.5 cumulative explosive growth during the heavy pollution episode (HPE) in 2016 Beijing wintertime, Tellus B: Chemical and Physical Meteorology, 71(1), DOI: 10.1080/16000889.2019.1620079, 2019.

Wu, L., Wang, Y., Li, L. and Zhang, G.: Acidity and inorganic ion formation in $PM_{2.5}$ based on continuous online observations in a South China megacity, Atmos. Pollut. Res., 11(8): 1339-1350, DOI: 10.1016/j.apr.2020.05.003, 2020.

Wu, L. Y., Tong, S. R., Wang, W. G. and Ge, M. F.: Effects of temperature on the heterogeneous oxidation of sulfur dioxide by ozone on calcium carbonate, Atmos. Chem. Phys., 11(13): 6593-6605, DOI: 10.5194/acp-11-6593-2011, 2011.

Xie, Y., Ding, A., Nie, W., Mao, H., Qi, X., Huang, X., Xu, Z., Kerminen, V.-M., Petäjä, T., Chi, X., Virkkula, A., Boy, M., Xue, L., Guo, J., Sun, J., Yang, X., Kulmala, M. and Fu, C.: Enhanced sulfate formation by nitrogen dioxide: Implications from in situ observations at the SORPES station, J. Geophys. Res.: Atmospheres, 120(24): 12679-12694, DOI: 10.1002/2015jd023607, 2015.

Xu, W., Kuang, Y., Liang, L., He, Y., Cheng, H., Bian, Y., Tao, J., Zhang, G., Zhao, P., Ma, N., Zhao, H., Zhou, G., Su, H., Cheng, Y., Xu, X., Shao, M. and Sun, Y.: Dust-Dominated Coarse Particles as a Medium for Rapid Secondary Organic and Inorganic Aerosol Formation in Highly Polluted Air, Environ Sci Technol, 54(24): 15710-15721, DOI: 10.1021/acs.est.0c07243, 2020.

Yu, F. and Luo, G.: Simulation of particle size distribution with a global aerosol model: contribution of nucleation to aerosol and CCN number concentrations, Atmos. Chem. Phys., 9: 7691–7710, 2009.

Zhang, Q., Zheng, Y., Tong, D., Shao, M., Wang, S., Zhang, Y., Xu, X., Wang, J., He, H., Liu, W., Ding, Y., Lei, Y., Li, J., Wang, Z., Zhang, X., Wang, Y., Cheng, J., Liu, Y., Shi, Q., Yan, L., Geng, G., Hong, C., Li, M., Liu, F., Zheng, B., Cao, J., Ding, A., Gao, J., Fu, Q., Huo, J., Liu, B., Liu, Z., Yang, F., He, K. and Hao, J.: Drivers of improved $PM_{2.5}$ air quality in China from 2013 to 2017, Proc Natl Acad Sci, 116(49): 24463-24469, DOI: 10.1073/pnas.1907956116, 2019.